Proc. Natl. Acad. Sci. USA
Vol. 96, pp. 7650–7657, July 1999
Colloquium Paper

This paper was presented at the National Academy of Sciences colloquium "The Neurobiology of Pain," held December 11–13, 1998, at the Arnold and Mabel Beckman Center in Irvine, CA.

Calcium regulation of a slow post-spike hyperpolarization in vagal afferent neurons

(spike frequency adaptation/ryanodine receptor/autacoids/allergic inflammation/mast cell)

RUTH CORDOBA-RODRIGUEZ*, KIMBERLY A. MOORE*, JOSEPH P. Y. KAO†, AND DANIEL WEINREICH*‡

*Department of Pharmacology and Experimental Therapeutics and †Medical Biotechnology Center and Department of Physiology, University of Maryland, School of Medicine, Baltimore, MD 21201-1559

ABSTRACT **Activation of distinct classes of potassium channels can dramatically affect the frequency and the pattern of neuronal firing. In a subpopulation of vagal afferent neurons (nodose ganglion neurons), the pattern of impulse activity is effectively modulated by a Ca^{2+}-dependent K^+ current. This current produces a post-spike hyperpolarization (AHP_{slow}) that plays a critical role in the regulation of membrane excitability and is responsible for spike-frequency accommodation in these neurons. Inhibition of the AHP_{slow} by a number of endogenous autacoids (e.g., histamine, serotonin, prostanoids, and bradykinin) results in an increase in the firing frequency of vagal afferent neurons from <0.1 to >10 Hz. After a single action potential, the AHP_{slow} in nodose neurons displays a slow rise time to peak (0.3–0.5 s) and a long duration (3–15 s). The slow kinetics of the AHP_{slow} are due, in part, to Ca^{2+} discharge from an intracellular Ca^{2+}-induced Ca^{2+} release (CICR) pool. Action potential-evoked Ca^{2+} influx via either L or N type Ca^{2+} channels triggers CICR. Surprisingly, although L type channels generate 60% of action potential-induced CICR, only Ca^{2+} influx through N type Ca^{2+} channels can trigger the CICR-dependent AHP_{slow}. These observations suggest that a close physical proximity exists between endoplasmic reticulum ryanodine receptors and plasma membrane N type Ca^{2+} channels and AHP_{slow} potassium channels. Such an anatomical relation might be particularly beneficial for modulation of spike-frequency adaptation in vagal afferent neurons.**

Activation and sensitization of primary afferent nerve fibers during allergic inflammation are orchestrated by inflammatory mediators released from various cells, including tissue mast cells. Inflammatory mediators provoke excitability changes in sensory nerves through diverse mechanisms, including (*i*) modification of the density and coupling efficacy of ligand-gated ionic channels; (*ii*) alteration in voltage-gated sodium, potassium, and calcium channels; and (*iii*) manipulation of cellular mechanisms that control spike-frequency adaptation.

After immunologic activation of mast cells in airway *in vivo* or in sensory ganglia *in vitro*, a wide range of electrophysiological changes can be detected in peripheral sensory nerve terminals of the vagus (1) and in vagal primary afferent somata (located in the nodose and jugular ganglia) (2). These changes range from transient (minutes) membrane depolarizations that sometimes reach action potential (AP) threshold (3) to a sustained (days) unmasking of functional NK-2 tachykinin receptors (4, 5). One electrical membrane property that is particularly sensitive to inflammatory mediators is a slow post-spike afterhyperpolarization (AHP_{slow}; see Fig. 1) (3). This slow afterpotential influences neuronal excitability and determines the frequency and pattern of neuronal discharge. We have found that the amplitude and duration of the AHP_{slow} are exquisitely sensitive to known inflammatory mediators such as prostanoids, amines, and kinins applied exogenously (Table 1) or released endogenously (i.e., after immunologic activation of mast cells) (3, 6). Inhibition of the AHP_{slow} is accompanied by a loss of spike-frequency adaptation. Thus, modulation of the AHP_{slow} amplitude and duration provides a mechanism for neuronal sensitization.

We are interested in identifying the ionic channels and second-messenger transduction pathways that participate in the initiation and maintenance of the AHP_{slow} in vagal primary afferent neurons. In this report, we describe the general properties of this slow afterpotential and our progress in its characterization. Our working hypothesis is that a close functional proximity between three separate channels [N type voltage-sensitive calcium channels, ryanodine (RY)-sensitive Ca^{2+}-induced Ca^{2+} release (CICR) calcium channels, and AHP_{slow} K^+ (SK) channels that underlie the AHP_{slow}] is essential for the initiation of the AHP_{slow}.

RESULTS

General Properties of Vagal Afferent AHP_{slow}. The AHP_{slow} is observed in a wide variety of peripheral and central neurons (for review, see ref. 7). In nodose neurons, AHP_{slow} is always preceded by a fast post-spike afterhyperpolarization (AHP_{fast}, 10–50 ms) that occurs at the end of the AP repolarization. In some neurons, the AHP_{fast} is followed by a second afterpotential that lasts 50–300 ms (AHP_{medium}). The AHP_{medium} is voltage- and Ca^{2+}- dependent and blocked by 10 mM tetraethylammonium in ≈50% of neurons, suggesting that it is mediated by large-conductance Ca^{2+}-activated K^+ channels (BK channels) (8).

In vagal afferent somata, the AHP_{slow} is particularly robust. After a single AP, the AHP_{slow} displays a delayed onset (100–500 ms), a slow rise time to peak (0.3–5 s), and a long duration (2–15 s; see Fig. 1). The proportion of AHP_{slow} neurons within nodose ganglia varies among species: ≈20% in the guinea pig, ≈35% in rabbit, and ≈85% in ferret. Only nodose neurons classified as C fibers (conduction velocity <1 m/s) possess AHP_{slow}. To date, there have been few species differences in the pharmacological or physiological properties

Abbreviations: AP, action potential; BK, large-conductance Ca^{2+}-activated K^+ channels; SK, small-conductance Ca^{2+} -activated K^+ channels; CICR, Ca^{2+}-induced Ca^{2+} release stores; RY, ryanodine; VDCC, voltage-dependent Ca^{2+} channels; L, N, R, L type, N type, and R-type VDCC; AHP, afterhyperpolarization; DBHQ, 2,5,-di(*t*-butyl)hydroquinone.

‡To whom reprint requests should be addressed. e-mail: dweinrei@umaryland.edu.

PNAS is available online at www.pnas.org.

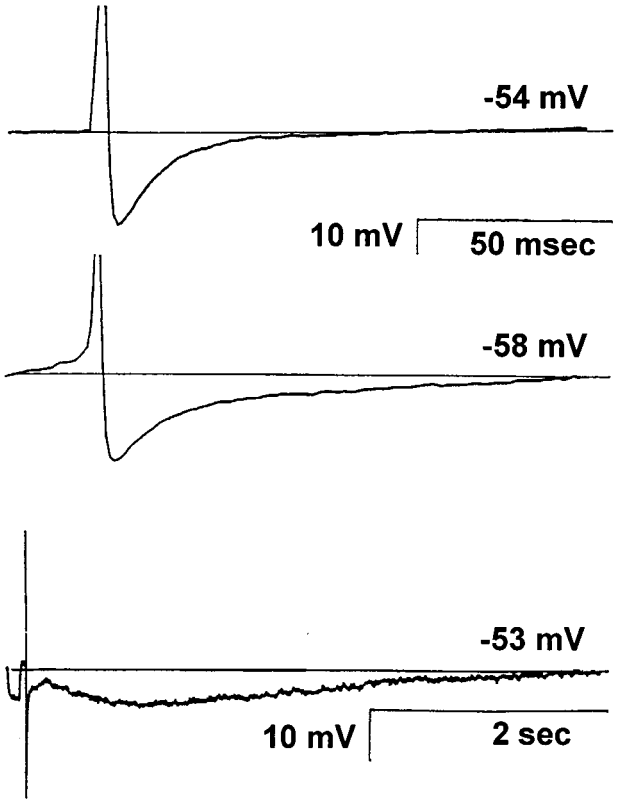

FIG. 1. A single AP can evoke three types of AHP in nodose neurons. (*Top*) A neuron with a single-component afterpotential lasting ≈30 ms. This AHP is designated AHP_{fast}. All neurons have this short duration afterpotential. (*Middle*) Example of a neuron with two afterpotentials, an AHP_{fast} followed by a longer lasting afterpotential (≈300 ms), the AHP_{medium}. In approximately half of the neurons, the AHP_{medium} is Ca^{2+}-dependent. (*Bottom*) In a subset of C fiber type nodose neurons, a slowly developing (hundreds of ms) and long-lasting (2–15 s) afterpotential is observed. This slow afterpotential (AHP_{slow}) is always Ca^{2+}-dependent. Intracellular recordings were obtained at room temperature from adult neurons isolated from rabbit nodose ganglia. The values near the horizontal lines are resting membrane potentials. The calibration in the *Top* also applies to the *Middle*. Similar results have been recorded in guinea pig and ferret nodose neurons.

of the AHP_{slow}. An analogous slow AHP has also been recently described in ≈25% of C type dorsal root ganglion neurons of the rat (9, 10).

The AHP_{slow} in vagal afferent neurons influences cellular excitability and controls AP frequency over the physiological range from 0.1 Hz to 10 Hz (11, 12). One interesting property of the AHP_{slow} is that its amplitude is tuned to both AP number and frequency. Over the range of 1–100 Hz, the amplitude of the AHP_{slow} increases with the number of APs until it plateaus after ≈15 APs (Fig. 2); similar results were observed when the current underlying the AHP_{slow} was monitored. For reasons still unresolved, 10 Hz (100-msec interspike intervals) consistently evokes the largest responses.

Table 1. Inflammatory mediators that block AHP_{slow} in vagal afferent neurons

Mediator	Receptor type	EC_{50}, nM
Bradykinin	B_2	72
Histamine	H_1	2,000
Serotonin	nd	300
PGD_2, PGE_2	nd	~20
Leukotriene C_4	nd	~100

Bradykinin (26), histamine (27), serotonin (28), PGD_2 and PGE_2 (12), and leukotriene C_4 (3) block the AHP_{slow}. nd, not determined; PG prostaglandin.

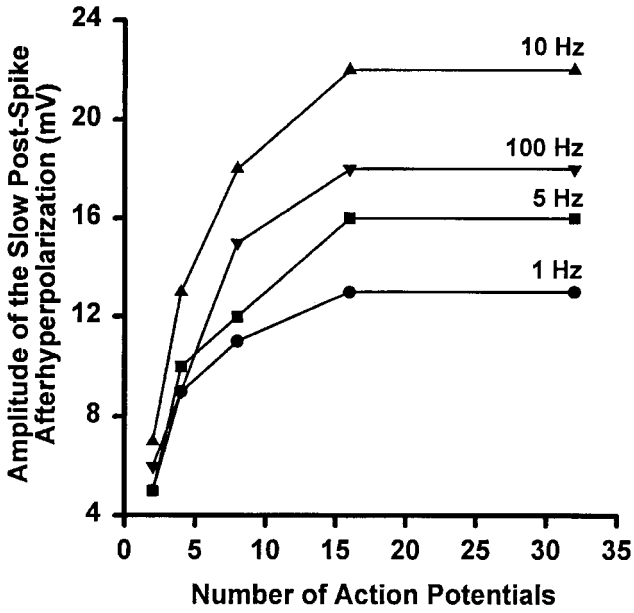

FIG. 2. Effects of varying numbers of APs and frequency on the amplitude of the AHP_{slow}. All data points were recorded from a single acutely dissociated adult rabbit nodose neuron at room temperature. Resting potential and membrane input resistance were −55 mV and 53 MΩ, respectively. APs were evoked by transmembrane depolarizing current pulses (2 nA, 3 ms) at the frequencies indicated. Similar results were obtained when measuring I_{AHP} by using the hybrid voltage-clamp technique in rabbit, guinea pig, and ferret nodose neurons.

The current generating the AHP_{slow} (I_{AHP}) is a voltage-insensitive Ca^{2+}-dependent K^+ current (13, 14) that is unaffected by a wide range of K^+ channel antagonists: 100 nM apamin, 10 μM *d*-tubocurarine, 5 mM Cs^+, 30 mM tetraethylammonium, 10 mM Ba^{2+}, 4 mM 4-aminopyridine, and 10 nM charybdotoxin. The magnitude of the AHP_{slow} (or the I_{AHP}) is linearly related to the concentration of extracellular Ca^{2+} (Fig. 3) and requires a rise in cytosolic free Ca^{2+} ($[Ca^{2+}]_i$) for activation. Buffering intracellular Ca^{2+} with 1,2-bis(2-aminophenoxy)ethane-*N,N,N′,N′*-tetraacetic acid (BAPTA) abolishes the AHP_{slow} (Fig. 4). Noise analysis of the I_{AHP} suggests a single-channel conductance of ≈10 pS (unpublished observations). These features are consistent with the properties of a small-conductance Ca^{2+}-activated K^+ channel (SK channel; ref. 8). Of the several SK channels recently cloned from mammalian brain (15), the hSK1 channel has a pharmacological and biophysical profile compatible with the K^+ current underlying the AHP_{slow} in nodose neurons.

Ca^{2+} Injection Evokes Two Temporally Distinct Outward Currents. To test whether the K^+ channels associated with the AHP_{medium} and the AHP_{slow} are directly activated by Ca^{2+}, we iontophoretically injected Ca^{2+} into nodose neurons. Independent of the AHP_{slow}, a large outward current with rapid activation and decay kinetics was elicited by Ca^{2+} injection. This current ($I_{K\text{-medium}}$) was evoked at holding potentials between −2 mV and −45 mV. It was completely blocked by 5 mM tetraethylammonium but unaffected by inhibitors of the AHP_{slow} (100 nM prostaglandins D_2 or E_2 or 1 μM forskolin). $I_{K\text{-medium}}$ was strongly voltage-dependent, requiring membrane holding potentials more positive than −55 mV. Assuming a reversal potential of −80 mV, $I_{K\text{-medium}}$ had an *e*-fold increase in peak conductance for each 8.0 ± 1.0 mV (mean ± SEM; n = 8) depolarization, as calculated from semilogarithmic plots of peak chord conductance versus voltage-clamp holding potential. These properties are similar to those of large-conductance BK (AHP_{medium}) channels.

In neurons that exhibited AHP_{slow}, Ca^{2+} injection provoked a slowly developing and protracted outward current ($I_{K\text{-slow}}$).

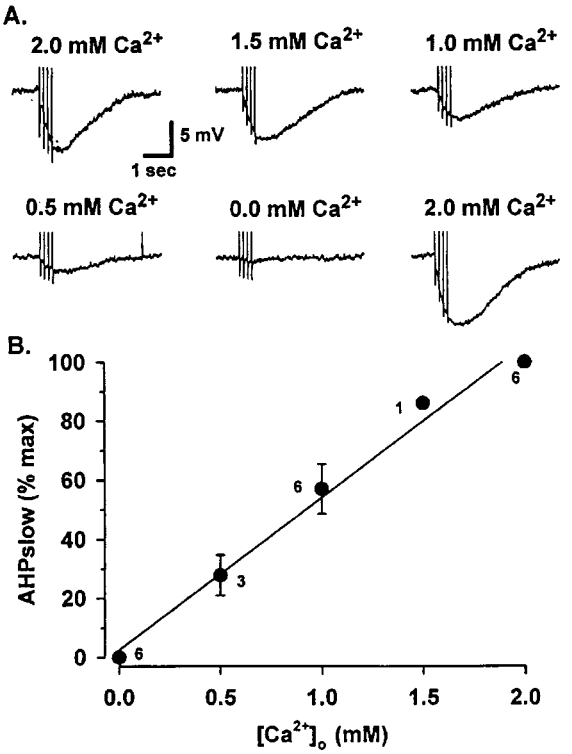

FIG. 3. Effects of varying $[Ca^{2+}]_o$ on the amplitude of the AHP_{slow} recorded in isolated nodose neurons. (*A*) Sample traces of AHP_{slow} evoked by a train of four APs in the presence of different $[Ca^{2+}]_o$. APs are evoked by transmembrane depolarizing current pulses (2 nA, 3 ms, 10 Hz) and are truncated. $[Ca^{2+}]_o$ was varied from 2.0 to 0.0 mM in 0.5 mM decrements. The AHP_{slow} is completely blocked when $[Ca^{2+}]_o$ is reduced to nominally zero. On returning to 2.0 mM $[Ca^{2+}]_o$, the AHP_{slow} recovers to its original amplitude. (*B*) Relation between $[Ca^{2+}]_o$ and AHP_{slow} amplitude recorded in several neurons. Values are means ± SEM of the number of observations indicated near each data point. Data are normalized to the maximum response recorded in a given neuron. Linear regression analysis yields the solid line (r = 0.993).

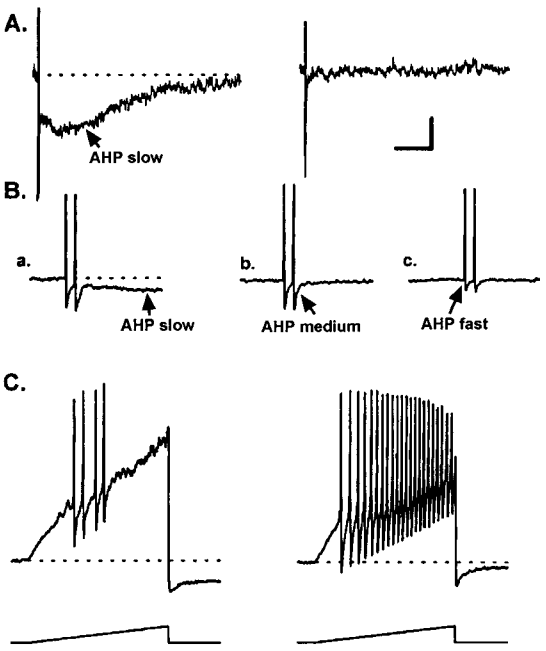

FIG. 4. Effects of BAPTA on the AHP_{slow} and on the excitability of an acutely dissociated rabbit nodose neuron. (*A*) Bath-applied BAPTA/acetomethylester (10 μM) blocks the AHP_{slow} within 5 min without changing the resting membrane potential or membrane input resistance. APs were evoked by transmembrane depolarizing current pulses (4 nA, 1.5 ms, 10 Hz) and are truncated. (*B*) Responses recorded at a faster sweep speed to illustrate the kinetics of the AHP_{fast} and AHP_{medium}, which precede the AHP_{slow}. The AHP_{fast} is unaffected by 10 μM BAPTA/acetomethylester (compare *a* with *b*). The Ca^{2+} dependence of the AHP_{medium} is illustrated in *c*, where the neuron is superfused with 100 μM $CdCl_2$ for 30 s, which blocks most of the AHP_{medium}. The residual component of the AHP recorded in $CdCl_2$ is the AHP_{fast}, which is mediated by delayed rectifier K^+ channels. (*C*) Depression of the AHP_{slow} markedly increases neuronal excitability. The average AP firing frequency induced by a current ramp protocol (1 nA, 2 s) increased from 1 to 5.5 Hz when the AHP_{slow} was blocked. Similar loss of spike-frequency adaptation was observed with bradykinin, prostaglandin D_2, histamine, and other inflammatory autacoids (see Table 2). The scale bar represents 3 mV, 2 s in *A*; 15 mV, 0.25 s in *B*; and 15 mV, 0.5 s in *C*. The dashed line represents the resting membrane potential (−60 mV). Resting membrane input resistance was 70 MΩ. Data is from ref. 19 with permission from the American Physiological Society.

Fig. 5 shows an overlay of the outward current responses evoked by Ca^{2+} injection in a single nodose C type neuron at holding potentials of −20 mV and −50 mV. The kinetic differences between $I_{K\text{-medium}}$ and $I_{K\text{-slow}}$ after Ca^{2+} injection are dramatic. In contrast to the rapid activation of $I_{K\text{-medium}}$, the onset of $I_{K\text{-slow}}$ is delayed, and the decay of $I_{K\text{-medium}}$ is nearly complete before the peak amplitude of the $I_{K\text{-slow}}$ is reached. These two outward currents mirror the temporal and pharmacological differences between AHP_{medium} and AHP_{slow}. $I_{K\text{-slow}}$, like the AHP_{slow}, was blocked by 100 nM prostaglandin D_2. The data shown in Table 2 summarize quantitative differences between these two Ca^{2+}-induced outward currents.

It is possible that the delayed onset of $I_{K\text{-slow}}$ compared with $I_{K\text{-medium}}$ results from unequal Ca^{2+} diffusion distances from the injection site to the two types of K^+ channels. This cause seems unlikely because the orientation of impalement was random, and the plasma membranes of dissociated nodose neurons appear devoid of processes that would provide semi-isolated regions where $I_{K\text{-slow}}$ might be generated. An alternative possibility is that additional intermediate steps, such as the synthesis or release of a second messenger, are required to activate $I_{K\text{-slow}}$. The large Q_{10} (>3.0; ref. 14) supports the latter alternative. One candidate is mobilization of intracellularly stored Ca^{2+}.

Ca^{2+} Released by the CICR Pool Is Essential for the Generation of the AHP_{slow}. Single APs produce transient increases in $[Ca^{2+}]_i$ (ΔCa_t) as measured by the fluorescent indicator fura-2. The magnitude of the ΔCa_t depends on both $[Ca^{2+}]_o$ and the number of APs. Over the range of one to eight APs, there is an approximately linear relation between the magnitude of the ΔCa_t and the number of APs (Fig. 6). In the presence of drugs that block CICR but do not significantly affect AP-induced Ca^{2+} influx [(RY, 10 μM), 2,5,-di(*t*-butyl)hydroquinone (DBHQ, 10 μM), or thapsigargin (TG, 100 nM)], we found that at least eight APs were required to evoke a detectable ΔCa_t (Fig. 6). In the presence of RY, DBHQ, and TG, the ΔCa_t–AP relation exhibits slopes of 0.5, 1.1, and 0.8 nM per AP, respectively. When compared with the slope of 9.6 nM per AP in control neurons, Ca^{2+} influx produced by a single nodose AP is amplified by 5- to 10-fold by CICR (16). Nodose neurons demonstrate a relatively low stimulus threshold for eliciting CICR. For instance, a robust CICR response can be observed after a single AP stimulus in nodose neurons, whereas many tens of APs are required in dorsal root ganglion neurons (17). The greater CICR response in nodose neurons is not due to greater Ca^{2+} influx through voltage-dependent Ca^{2+} channels (VDCCs); a single AP produces comparable Ca^{2+} influx in nodose and dorsal root ganglion neurons (39 vs. 49 pC, respectively; refs. 16 and 18). Rather, the more responsive CICR pool in nodose neurons

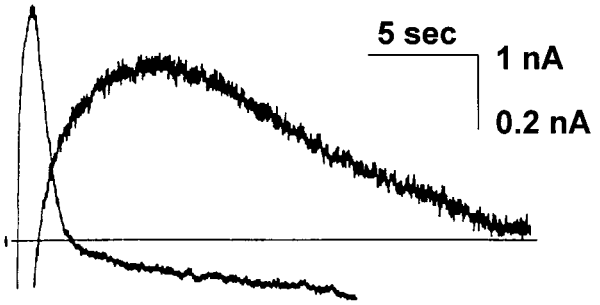

FIG. 5. Comparison of two outward K^+ currents evoked by intracellular Ca^{2+} injection. Recordings were made in a single acutely isolated adult rabbit nodose neuron. A slow outward current ($I_{K\text{-slow}}$) was activated by a 5-nA, 1-s iontophoretic Ca^{2+} injection at a holding potential of −50 mV. A second outward current ($I_{K\text{-medium}}$) was activated at −20 mV (5 nA, 0.5 sec). $I_{K\text{-medium}}$ activates and decays completely before $I_{K\text{-slow}}$ reaches peak amplitude. $I_{K\text{-medium}}$ was blocked by 10 mM tetraethylammonium; $I_{K\text{-slow}}$ was blocked by 100 nM prostaglandin D_2. The iontophoretic pipette was filled with a 0.2 M $CaCl_2$ solution. Voltage-clamp currents were recorded with a second intracellular pipette. The discontinuous (switched) current injection mode of an Axoclamp II amplifier was used for both current- and voltage-clamp applications. The larger calibration value is for $I_{K\text{-medium}}$. Population data is shown in Table 2.

may reflect either a closer proximity between plasma membrane Ca^{2+} influx channels and endoplasmic reticulum RY receptors or a more sensitive RY receptor.

By using physiological stimuli (APs) in conjunction with pharmacological manipulations of CICR, we have demonstrated that CICR is essential for the development of the AHP_{slow}. Over the range of 1–16 APs, the magnitudes of the AP-induced AHP_{slow} and the ΔCa_t (a monitor of CICR in these neurons) were highly correlated ($r = 0.985$). Simultaneous recordings of ΔCa_t and AHP_{slow} before and during bath application of CICR inhibitors (RY, TG, DBHQ, or 10 μM cyclopiazonic acid) revealed that both responses were blocked in a parallel fashion (Fig. 7; see also Table 1 in ref. 19). These data indicate that a CICR pool is essential for the generation of the AHP_{slow}. They also provide a potential explanation for the slow kinetics of the AHP_{slow}, namely Ca^{2+} mobilization from CICR.

Effects of Changing $[Ca^{2+}]_o$ on the AHP_{slow}, ΔCa_t, and Ca^{2+} influx. If the AHP_{slow} depends on Ca^{2+} released from the CICR pool triggered by AP-induced Ca^{2+} influx, it would follow that changes in $[Ca^{2+}]_o$ should produce corresponding effects on both the AHP_{slow} and the ΔCa_t. The data shown in Fig. 3*A* illustrate the effects of progressively lowering $[Ca^{2+}]_o$ from 2.0 mM to nominally zero on the amplitude of the AHP_{slow} recorded in a single nodose neuron. As $[Ca^{2+}]_o$ was decreased, the amplitude of the AHP_{slow} was reduced proportionally. When the results from this and five additional neurons were plotted (Fig. 3*B*), the relation between $[Ca^{2+}]_o$ and the amplitude of the AHP_{slow} was linear ($r = 0.993$; $n = 6$, pooled data from three current-clamp and three hybrid voltage-clamp experiments).

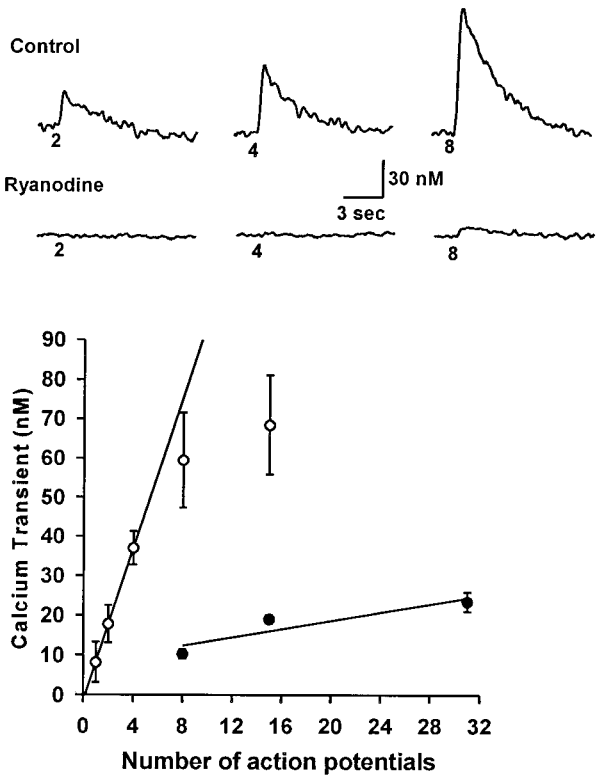

FIG. 6. (*Upper*) Effect of RY on AP-induced Ca^{2+} transients. Traces are Ca^{2+} transients evoked by varying numbers of APs, as indicated below each trace. In control neurons, distinct Ca^{2+} transients can be elicited by very few APs. In contrast, in the presence of 10 μM RY, a CICR inhibitor, at least eight APs are required to generate a discernible change in $[Ca^{2+}]_i$. Suppression of the Ca^{2+} transient by RY is due to its effect on CICR and not the result of nonspecific effects on Ca^{2+} channels; the kinetics and amplitude of I_{Ca} elicited by APs are completely unaffected by RY. (*Lower*) Effect of RY on the relation between the amplitude of Ca^{2+} transients and number of APs. ○ and ● are mean amplitudes of Ca^{2+} transients evoked by varying numbers of action potentials for control ($n = 10$) and for RY-treated nodose neurons ($n = 3$), respectively. Linear regression of data from control (≤4 action potentials) and RY-treated cells yielded slopes of 9.6 ± 0.01 and 0.5 ± 0.23 nM per AP, respectively. Comparison of the slopes illustrates that CICR is capable of amplifying the "trigger" Ca^{2+} resulting from AP-induced Ca^{2+} influx by 20-fold. Data is modified from ref. 16 with permission from *Journal of Physiology (London)*.

Next, we examined the relation between $[Ca^{2+}]_o$ and the magnitude of the AP-induced ΔCa_t. Fig. 8*A* illustrates ΔCa_ts elicited by varying numbers of APs recorded from a single neuron in Locke solution containing 2.2 or 1.1 mM Ca^{2+}. The population results relating the normalized amplitude of the ΔCa_ts recorded in four neurons to the number of APs is shown in Fig. 8*B*. In 1.1 mM $[Ca^{2+}]_o$, the first few APs did not elicit a measurable ΔCa_t. For the neuron shown in Fig. 8*A*, at least eight APs were necessary to evoke a detectable ΔCa_t. In three additional neurons, the minimum number of APs necessary to

Table 2. Comparison of $I_{K\text{-slow}}$ and $I_{K\text{-medium}}$

Current	Peak conductance, nS	*n*	Holding potential, mV	*n*	Time-to-peak, ms	*n*	Decay time constant, ms	*n*	Duration, s	*n*
$I_{K\text{-slow}}$	27.9 ± 6.5	14	−55.4 ± 2.7	14	6,570 ± 1085	12	6,735 ± 789	5	23 ± 3.4	14
$I_{K\text{-medium}}$	53.2 ± 16.5	6	−20 ± 3.7	6	958 ± 56	6	818 ± 97	6	2.5 ± 0.16	6

$I_{K\text{-slow}}$ and $I_{K\text{-medium}}$ are outward currents elicited by iontophoretic injection Ca^{2+} into acutely isolated nodose neurons of the rabbit. The peak conductance is the largest conductance elicited, independent of membrane potential. The holding potential is the potential at which the peak conductance was measured. The decay time constant was measured by fitting a line, by eye, to the log transform of the decay of the current. The duration was calculated from the onset of Ca^{2+} injection to the time at which the current had decayed to 20% of its peak value. Data are summarized as the mean ± SEM.

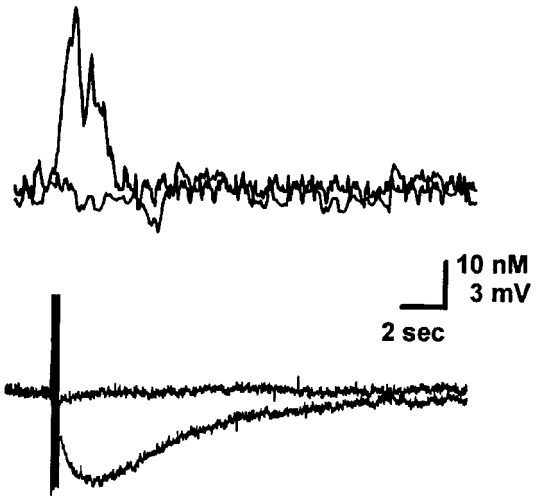

FIG. 7. Effect of DBHQ, a functional CICR inhibitor, on the AP-induced Ca^{2+} transient and on the AHP_{slow} recorded simultaneously in an acutely isolated rabbit nodose neuron. *Upper* traces represent superimposed Ca^{2+} transients evoked by a train of four APs (10 Hz) recorded in control Locke solution and 7 min after switching to Locke solution containing 10 μM DBHQ. The lower pair of traces shows AHP_{slow}. DBHQ treatment completely blocked both the Ca^{2+} transient and the AHP_{slow}. Resting $[Ca^{2+}]_i$ was 91 nM. Fluorescence data were acquired at 10 Hz. Resting membrane potential was −67 mV. AP amplitudes are truncated. Data are from ref. 19 with permission from the American Physiological Society.

elicit a detectable ΔCa_t ranged from 4 to 32. The ΔCa_t–AP relation recorded in 1.1 mM $[Ca^{2+}]_o$, as in Locke solution containing normal $[Ca^{2+}]_o$, followed a hyperbolic relation (χ^2 = 6.75 and 0.31; r = 0.988 and 0.999 for 2.2 and 1.1 mM Ca^{2+},respectively; Fig. 8*B* and see also Fig. 1 in ref. 16). Given the hyperbolic nature of the ΔCa_t–AP relation, deducing the effects of altered $[Ca^{2+}]_o$ on the magnitude of the ΔCa_t clearly depends on where along this relation the comparison is made. At one extreme, there is a ≈2-fold change when comparing the plateau phases of the curves in normal and one-half normal $[Ca^{2+}]_o$. It is also possible to calculate the limiting initial slopes for the rising phase of the curves (dashed lines in Fig. 8*B*). The limiting slopes, which represent the full Ca^{2+} release potential of the CICR pool before any release has actually occurred, were 15 ± 3.8 and 2 ± 0.7 nM per AP in 2.2 and 1.1 mM $[Ca^{2+}]_o$, respectively. Thus, reducing $[Ca^{2+}]_o$ by a factor of 2 results in a reduction of the ΔCa_t by a factor of 7 ± 2.8 when the rising phases of the two curves are compared. The ≈7-fold reduction of the ΔCa_t associated with halving $[Ca^{2+}]_o$ is much larger than the 2-fold reduction in the AHP_{slow} amplitude (Fig. 3), suggesting that some, but not all, of the Ca^{2+} released from the CICR pool is required for the generation of the AHP_{slow}.

The disproportionate effect of reduced $[Ca^{2+}]_o$ on the ΔCa_t versus the AHP_{slow} could arise from a nonlinear reduction of Ca^{2+} influx per AP and/or from a decreased Ca^{2+} release from CICR pool per unit Ca^{2+} influx. To study these possibilities, we examined the effect of lowering $[Ca^{2+}]_o$ on AP-induced Ca^{2+} influx. The amount of Ca^{2+} entering a neuron with each AP in normal and in reduced $[Ca^{2+}]_o$ was determined by using a prerecorded AP as whole-cell voltage-clamp command under experimental conditions where the major inward charge carrier is Ca^{2+} (for details, see Fig. 2 in ref. 16). When $[Ca^{2+}]_o$ was decrementally reduced from 2 mM to nominally zero, the magnitude of the I_{Ca} decreased proportionally. The charge movement caused by Ca^{2+} influx, normalized to cell membrane capacitance (pC/pF), was plotted against varying $[Ca^{2+}]_o$ for 12 neurons. Over the range of 0–2.0 mM $[Ca^{2+}]_o$, Ca^{2+} influx varied linearly with $[Ca^{2+}]_o$ (r = 0.974). These results indicate that changes in Ca^{2+} influx alone

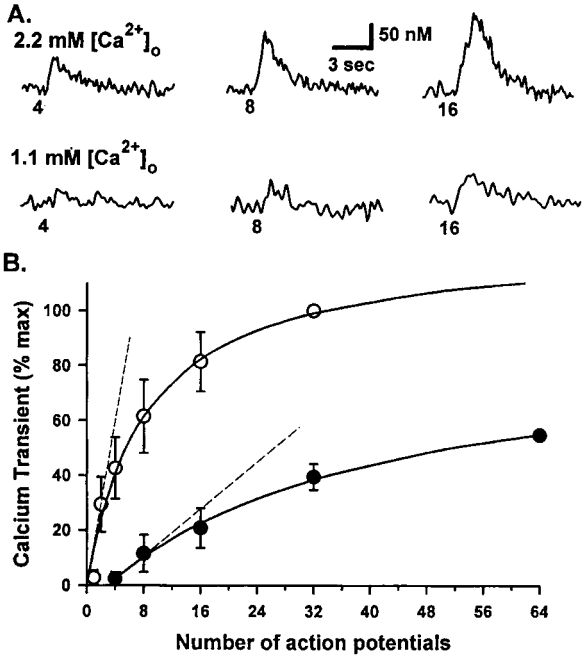

FIG. 8. Effect of varying $[Ca^{2+}]_o$ on the amplitude of AP -induced Ca^{2+} transients. (*A*) Representative traces of Ca^{2+} transients evoked by varying numbers of APs in normal (2.2 mM) and reduced (1.1 mM) $[Ca^{2+}]_o$. APs were elicited by transmembrane depolarizing current pulses (2 nA, 1.5 ms, 10 Hz). The number of APs is indicated below each trace. (*B*) The normalized (mean ± SEM) amplitude of Ca^{2+} transients recorded in four neurons is plotted against varying numbers of APs. Data are normalized to the maximal response recorded in a given neuron. ○ represents Ca^{2+} transients recorded in 2.2 mM $[Ca^{2+}]_o$; ● represents Ca^{2+} transients recorded in the same neurons in 1.1 mM $[Ca^{2+}]_o$. Continuous curves are rectangular hyperbolas fit to the data (χ^2 = 6.75 and 0.31, r = 0.988 and 0.999 for 2.2 and 1.1 mM $[Ca^{2+}]_o$, respectively). The dashed lines represent the limiting initial slopes (15 ± 3.8 and 2 ± 0.7 nM per AP for 2.2 and 1.1 mM $[Ca^{2+}]_o$, respectively).

cannot account for the disproportionate reduction in the ΔCa_t relative to the AHP_{slow} that is observed when $[Ca^{2+}]_o$ is reduced.

The disproportionate effect of reduced $[Ca^{2+}]_o$ on the ΔCa_t–AHP_{slow} relation could arise from a diminution in the amount of Ca^{2+} released from the CICR pool. Caffeine, a known agonist of CICR, is traditionally used to assess the releasable content of the CICR pool. In 8 of the 13 neurons studied, halving $[Ca^{2+}]_o$ reduced the caffeine-induced ΔCa_t by 20–79% (100% vs. 47 ± 7.2% in 2.2 and 1.1 mM $[Ca^{2+}]_o$, respectively; P = 0.0002). In other words, decreasing $[Ca^{2+}]_o$ by a factor of 2 caused a 1.25- to 5-fold reduction in the caffeine response. On returning to normal Locke solution, the caffeine response was restored to near control values. In the remaining five neurons, the caffeine-induced ΔCa_t was unaffected by reducing $[Ca^{2+}]_o$ (100% vs. 112 ± 8.4% in 2.2 and 1.1 mM $[Ca^{2+}]_o$, respectively; P = 0.690). There was no significant difference in resting levels of $[Ca^{2+}]_i$ between these two groups of neurons (93 ± 29.5 nM vs. 111 ± 29.7 nM; P = 0.530). Unfortunately, the wide variability in the effects of reduced $[Ca^{2+}]_o$ on the caffeine responses prevents a meaningful interpretation of the effect of $[Ca^{2+}]_o$ on the releasable content of the CICR pool.

Ca^{2+} Influx Through N Type Calcium Channels Selectively Elicits AHP_{slow}. Six types of VDCCs have been described in neurons: L, N, P, Q, R, and T (20). Nodose neurons express several types of VDCCs. By using a panel of pharmacologic reagents that are selective for different types of VDCCs, we tested the contribution of each to the total AP-induced Ca^{2+} current. Our results, summarized in Table 3, reveal that ≈85%

Table 3. Effects of Ca^{2+} channel blockers on action potential-induced inward Ca^{2+} currents

Channel type	Channel blocker	Concentration μM	Reduction	*n*
T	Amiloride	500	0 ± 0	18
L	Nifedipine	10	44 ± 5.6	9
P/Q	ω-AGA IVA	0.2	0 ± 0	2
Q	ω-CTX MVIIC	0.25	0 ± 0	6
N	ω-CTX GVIA	1	40 ± 4.0	15

The blocking effect of amiloride, nifedipine, ω-agatoxin (AGA) IVA, ω-conotoxin (CTX) MVIIC, and ω-conotoxin (CTX) GVIA is expressed as percent reduction in the peak amplitude of the total calcium current ± SEM. *n* corresponds to the number of cells for each condition.

of the AP-induced inward Ca^{2+} current is shared by L and N type Ca^{2+} channels (Fig. 9). P, Q, and T type Ca^{2+} channel antagonists were ineffective, suggesting that the remaining Ca^{2+} current is associated with Ca^{2+} influx through R type channels. Nifedipine (10 μM), an L type Ca^{2+} channel blocker, produced no measurable effect on either the AHP_{fast}, the AHP_{medium}, or the AHP_{slow}. By contrast, ω-conotoxin-GVIA (0.5 μM), a selective N type Ca^{2+} channel blocker, always

Table 4. Actions of specific Ca^{2+} channel blockers on the action potential-induced Ca^{2+} transient and the AHP_{slow}

Channel type	Channel blocker	Reduction, % Ca^{2+} transient	*n*	AHP_{slow} amplitude	*n*
L	Nifedipine	57 ± 7.7	21	0 ± 0	5
N	ω-CTX GVIA	39 ± 6.2	4	100 ± 0	6
T, R	Nickel	nd		0 ± 0	5
All	Cadmium	100 ± 0	2	100 ± 0	6

The following concentrations of antagonists were used: nifedipine (10 μM), ω-conotoxin GVIA (0.5 μM or 1 μM), nickel (50–500 μM), and cadmium (100 μM). nd, not determined.

obliterated the AHP_{slow}, and in ≈50% of the neurons abolished the AHP_{medium} (about half of the AHP_{medium} are Ca^{2+}-sensitive, see above), while leaving the AHP_{fast} unaffected (Fig. 9 and Table 4.). These results indicate that the SK and BK type K^+ channels are both regulated by Ca^{2+} influx through N type channels. BK channels are gated by influx Ca^{2+} directly (8), whereas SK channels are affected by influx Ca^{2+} indirectly (i.e., Ca^{2+} entering through N type VDCC triggers RY receptors to release Ca^{2+} from CICR pools). Such a sequence implies a functional coupling between N type Ca^{2+} channels

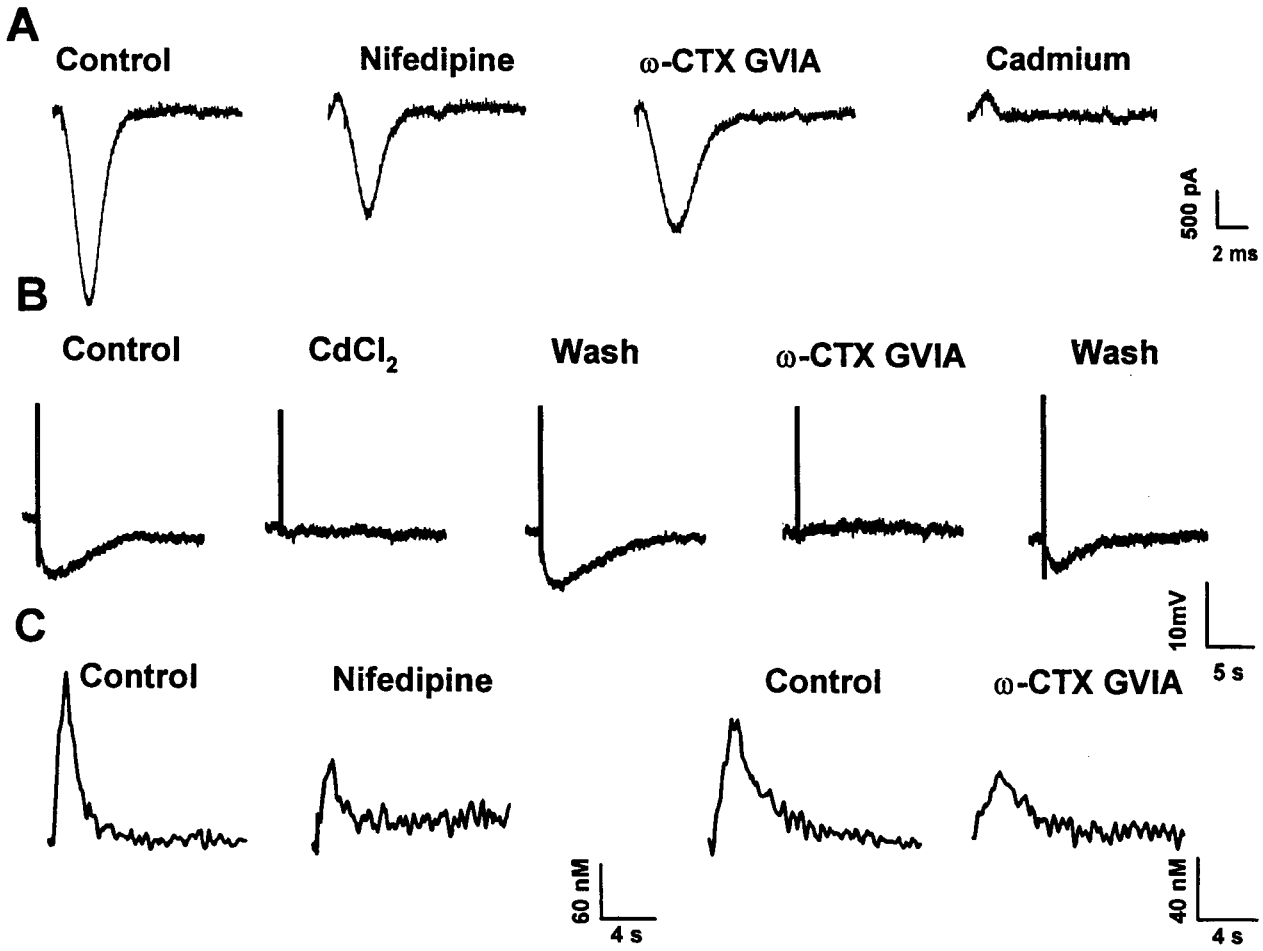

FIG. 9. Effects of VDCC antagonists on AP-induced calcium currents, AHP_{slow} and AP-induced Ca^{2+} transients. (*A*) Inward calcium currents recorded in isolated nodose neurons evoked by a prerecorded AP waveform from a holding potential of −60 mV. From *Left* to *Right*, control inward current in the presence of 2 mM $[Ca^{2+}]_o$ and in the presence of 10 μM nifedipine. After reestablishing control conditions, the neuron was exposed to 1 μM ω-conotoxin-GVIA. The effects of 500 μM cadmium were recorded in another neuron; the control current for this cell was similar to the first trace. (*B*) AHP_{slow} evoked by a train of four APs (10 Hz) recorded in another nodose neuron. From *Left* to *Right*, AHP_{slow} evoked in control conditions, in the presence of 100 μM $CdCl_2$, after washout, in the presence of 500 nM ω-conotoxin-GVIA, and after washout. (*C*) AP-induced Ca^{2+} transients recorded in two nodose neurons. From *Left* to *Right*, Ca^{2+} transients evoked by a train of eight APs in normal Locke solution, and in Locke solution containing 10 μM nifedipine. In another neuron, 1 μM ω-conotoxin-GVIA reduced the Ca^{2+} transient ≈50% (see Table 4). APs were evoked by 2.5-ms, 10-Hz depolarizing current pulses.

and RY channels in the endoplasmic reticulum. We tested this proposition by examining the effects of VDCC antagonists on the magnitude of AP-induced ΔCa_t.

Ca^{2+} influx through both L and N type Ca^{2+} channels triggers CICR. The magnitude of the ΔCa_t is a sensitive indicator of Ca^{2+} release from the CICR pool. To determine the relative influence of Ca^{2+} influx through L and N type channels on release from the CICR pool, we applied selective VDCC antagonists and monitored the amplitude of ΔCa_t. Nifedipine (10 μM) and ω-conotoxin-GVIA (0.5–1.0 μM) diminished the amplitude of the ΔCa_t by 57% and 39%, respectively (Fig. 9 and Table 4). These results reveal that Ca^{2+} entering through either L or N type Ca^{2+} channels provides "trigger" Ca^{2+} to stimulate CICR. Given that the amount of Ca^{2+} influx through L and N type Ca^{2+} channels is comparable (44% and 40%, respectively, of total AP-induced Ca^{2+} influx; see Table 3), there must be a remarkable spatial arrangement between plasma membrane N type Ca^{2+} channels, endoplasmic reticulum RY receptors, and plasma membrane SK channels. Our working hypothesis concerning the regulation of the AHP_{slow} by Ca^{2+} is illustrated schematically in Fig. 10.

DISCUSSION

Whether recorded in intact vagal sensory ganglia or in acutely isolated vagal afferent somata (nodose neurons), single APs can elicit an AHP_{slow} that exhibits a delayed onset (50–300 ms), a slow time to peak amplitude (0.3–0.5 s), and a particularly long duration (2–15 s) (14, 21). Inhibition of the AHP_{slow} by numerous inflammatory mediators (e.g., bradykinin, prostanoids, histamine, serotonin, leukotriene C_4; see Table 1) results in an increased neuronal excitability and a loss of spike-frequency adaptation. Thus, modulation of the AHP_{slow} by these mediators provides a mechanism for peripheral nociceptor sensitization that may underlie allergic inflammation-induced hyperalgesia.

One unresolved but important mechanistic question revolves around the delayed onset and protracted duration of the AHP_{slow}. Many of our studies of nodose AHP_{slow} were performed with acutely dissociated adult neurons, which are essentially spherical structures lacking dendritic and axonal processes. Thus, the delayed onset of the AHP_{slow} cannot be due to slow diffusion of Ca^{2+} from distal sites of influx to somal SK channels. The high temperature coefficient ($Q_{10} > 3.0$) for the rising phase and the decay time constant of the nodose AHP_{slow} (14) also argues against simple Ca^{2+} diffusion as an explanation for the slow kinetics of the AHP_{slow}. The time course of the AHP_{slow} could arise from unusual channel kinetics of the SK channels. This also appears unlikely if SK channels in nodose neurons have activation kinetics similar to those cloned from rat brain (22). Recombinant SK channels from rat brain have activation time constants that are orders of magnitude shorter than the rise time of the AHP_{slow}. It is more likely that the time course of the AHP_{slow} is a consequence of the ΔCa_t because of CICR.

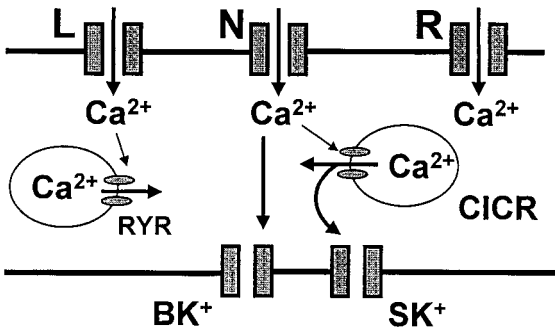

FIG. 10. Schematic diagram of the relation between plasma membrane Ca^{2+} channels, BK, and SK potassium channels and endoplasmic reticulum RY receptors in primary vagal afferent neurons. Single APs evoke Ca^{2+} influx through L and N type VDCCs. Ca^{2+} influx through either of these channels can trigger release of Ca^{2+} from the endoplasmic reticulum via RY receptors. Whereas BK channels are activated directly by Ca^{2+} entering the neuron via N type VDCC, SK channels are activated indirectly. SK channels require Ca^{2+} from CICR pools released after Ca^{2+} influx through N type channels.

If the AHP_{slow} is directly dependent on Ca^{2+} released from the CICR pool, the AHP_{slow} and the AP-induced rise in $[Ca^{2+}]_i$ should display similar kinetics. Quantitative kinetic comparisons between these two variables are subject to some uncertainty, because the time course of the ΔCa_t reflects global changes in $[Ca^{2+}]_I$, whereas the kinetics of the AHP_{slow} are determined by events at the plasma membrane. Nonetheless, we determined the time-to-peak and 10-to-90% decay time for both the AHP_{slow} and the ΔCa_t elicited by one to eight APs (19). The time-to-peak for AHP_{slow} was significantly slower than the ΔCa_t by nearly a factor of a two (1.0 s vs. 1.9 s); the ΔCa_t also decayed more rapidly than the AHP_{slow} (3 s vs. 7 s). Analogous temporal discrepancies have been reported between the ΔCa_t and AHP_{slow} in vagal motoneurons (23). Such temporal differences suggest that Ca^{2+} released from CICR pools does not act alone to gate AHP_{slow} K^+ channels. Cloned SK channels contain many potential phosphorylation sites (15); Ca^{2+}-dependent phosphorylation and/or dephosphorylation may thus be additional processes in the signal-transduction pathway of AP-evoked AHP_{slow}.

Unambiguous data now exist showing that Ca^{2+} can directly activate SK channels in hippocampal neurons (24) and in *Xenopus* oocytes (22). In nodose neurons, it is less clear whether Ca^{2+} alone is sufficient to activate and sustain the AHP_{slow} after an AP. In hippocampal neurons, flash photolysis of a "caged" Ca^{2+} chelator immediately truncates AP-induced AHP_{slow}, suggesting that elevated intracellular Ca^{2+} is required to maintain the AHP_{slow} (25). These results do not, however, distinguish between continuous Ca^{2+} gating of SK channel and the involvement of other Ca^{2+}-dependent factors sustaining the longevity of the AHP_{slow}. It is also possible that Ca^{2+}-dependent factors act synergistically with Ca^{2+} to control SK channels (23). The nearly spherical morphology and large size of acutely isolated adult nodose neurons provide a favorable preparation to determine the nature of second messengers required to activate and sustain the AHP_{slow}.

In conclusion, a subset of vagal primary afferent neurons possess a slowly developing and long-lasting spike afterhyperpolarization, the AHP_{slow}, that can profoundly affect the discharge frequency of these visceral afferent neurons. Although AP-evoked Ca^{2+} influx via both L and N type Ca^{2+} channels triggers CICR, only Ca^{2+} flux through N type channels activates the CICR-dependent AHP_{slow}. This type of specificity suggests that spatial coupling between N type Ca^{2+} channels and SK channels may be critical for the generation of the AHP_{slow} in nodose neurons. The exact mechanism coupling ΔCa_t to the AHP_{slow} current remains to be determined.

We thank our coworkers who participated in many of the experiments described in this manuscript: Drs. Akiva Cohen, Samir Jafri, and Bill Wonderlin, and Mr. Glen Taylor. The authors also thank Dr. Liz Katz and Mr. Eric Lancaster for their constructive suggestions on an earlier draft of this manuscript. This work was supported by National Institutes of Health Grants GM-46956 to J.P.Y.K., NS-22069 to D.W. and Training Grant NS-07375 to K.A.M.

1. Undem, B. J. & Riccio, M. M. (1997) in *Asthma*, eds. Barnes, P. J., Grunstein, M. M., Leff, A. & Woolcock, A. J. (Lippincott, Philadelphia), pp. 1009–1026.
2. Weinreich, D. (1995) *Pulm. Pharmacol.* **8,** 173–179.
3. Undem, B. J., Hubbard, W. & Weinreich, D. (1993) *J. Auton. Nerv. Syst.* **44,** 35–44.

4. Weinreich, D., Moore, K. A. & Taylor, G. E. (1997) *J. Neurosci.* **17,** 7683–7693.
5. Moore, K. A., Taylor, G. E. & Weinreich, D. (1999) *J. Physiol. (London)* **514.1,** 111–124.
6. Greene, R., Fowler, J. C., MacGlashlan, D., Jr. & Weinreich, D. (1988) *J. Appl. Physiol.* **64,** 2249–2253.
7. Sah, P. (1996) *Trends Neurosci.* **19,** 150–154.
8. Blatz, A. L. & Magleby, K. L. (1987) *Trends Neurosci.* **10,** 463–467.
9. Gold, M. S., Shuster, M. J. & Levine, J. D. (1996) *Neurosci. Lett.* **205,** 161–164.
10. Villière, V. & McLachlan, E. M. (1996) *J. Physiol. (London)* **76,** 1924–1941.
11. Coleridge, J. C. G. & Coleridge, H. M. (1984) *Rev. Physiol. Biochem. Pharmacol.* **99,** 1–110.
12. Weinreich, D. & Wonderlin, W. F. (1987) *J. Physiol. (London)* **394,** 415–427.
13. Higashi, H., Morita, K. & North, R. A. (1984) *J. Physiol. (London)* **355,** 479–492.
14. Fowler, J. C., Greene, R. & Weinreich, D. (1985) *J. Physiol. (London)* **365,** 59–75.
15. Köhler, M., Hirschberg, B., Bond, C. T., Kinzie, J. M., Marrion, N. V. & Adelman, J. P. (1996) *Nature (London)* **273,** 1709–1714.
16. Cohen, A. S., Moore, K. A., Bangalore, R., Jafri, M. S., Weinreich, D. & Kao, J. P. Y. (1997) *J. Physiol. (London)* **499,** 315–328.
17. Shmigol, A., Verkhratsky, A. & Isenberg, G. (1995) *J. Physiol. (London)* **489,** 627–636.
18. Scroggs, R. S. & Fox, A. P. (1992) *J. Neurosci.* **12,** 1789–1801.
19. Moore, K. A., Cohen, A. S., Kao, J. P. Y. & Weinreich, D. (1998) *J. Neurophysiol.* **79,** 688–694.
20. Dunlap, K., Luebke, J. I. & Turner, T. J. (1995) *Trends Neurosci.* **18,** 89–98.
21. Leal-Cardosa, H., Koschorke, G. M., Taylor, G. & Weinreich, D. (1993) *J. Auton. Nerv. Syst.* **45,** 29–39.
22. Hirschberg, B., Maylie, J., Adelman, J. P. & Marrion, N. V. (1998) *J. Gen. Physiol.* **111,** 565–581.
23. Lasser-Ross, B., Ross, W. N. & Yarom, Y. (1997) *J. Neurophysiol.* **78,** 825–834.
24. Marrion, N. V. & Tavalin, S. J. (1998) *Nature (London)* **395,** 900–905.
25. Lancaster, B. & Zucker, R. S. (1994) *J. Physiol. (London)* **475,** 229–239.
26. Weinreich, D., Koschorke, G. M., Undem, B. J. & Taylor, G. E. (1995) *J. Physiol. (London)* **483.3,** 735–746.
27. Jafri, M. S., Moore, K. A., Taylor, G. E. & Weinreich, D. (1997) *J. Physiol. (London)* **503.3,** 533–546.
28. Christian, E. P., Taylor, G. E. & Weinreich, D. (1989) *J. Appl. Physiol.* **67,** 584–591.